Journal of Power Sources 273 (2015) 413–422

Contents lists available at ScienceDirect

Journal of Power Sources

journal homepage: www.elsevier.com/locate/jpowsour

New charging strategy for lithium-ion batteries based on the integration of Taguchi method and state of charge estimation

Thanh Tu Vo, Xiaopeng Chen, Weixiang Shen*, Ajay Kapoor

Faculty of Science, Engineering and Technology, Swinburne University of Technology, Hawthorn, Victoria, 3122, Australia

HIGHLIGHTS

- New charging strategy is proposed based on integration of Taguchi method and stage of charge estimation.
- Optimal charging current pattern is determined using multiple-response optimisation technique in Taguchi method.
- Experiments of lithium ion batteries verify the effectiveness of the new charging strategy.
- New charging strategy has better performances than conventional constant current constant voltage charging method.

ARTICLE INFO

Article history:
Received 10 July 2014
Received in revised form
8 September 2014
Accepted 16 September 2014
Available online 28 September 2014

Keywords:
Optimal charging current pattern
Taguchi method
Adaptive switching gain sliding mode observer
State of charge estimation
Lithium polymer batteries

ABSTRACT

In this paper, a new charging strategy of lithium-polymer batteries (LiPBs) has been proposed based on the integration of Taguchi method (TM) and state of charge estimation. The TM is applied to search an optimal charging current pattern. An adaptive switching gain sliding mode observer (ASGSMO) is adopted to estimate the SOC which controls and terminates the charging process. The experimental results demonstrate that the proposed charging strategy can successfully charge the same types of LiPBs with different capacities and cycle life. The proposed charging strategy also provides much shorter charging time, narrower temperature variation and slightly higher energy efficiency than the equivalent constant current constant voltage charging method.

1. Introduction

The use of portable electronic devices has been significantly increased in recent years. The traditional rechargeable batteries such as lead-acid, nickel–cadmium and nickel-metal hydride batteries used in these devices have tended to be replaced with lithium-ion batteries, which exhibit several appealing features of high power and energy densities, broad operating temperature range, long life cycles, no memory effect and low self-discharge rate [1–3]. The merits of these lithium-ion batteries also meet high-energy demand of electric vehicles (EVs), making them as very promising primary power sources for EVs in the future [4]. For the applications of lithium-ion batteries, a well-designed battery charger plays a vital role for sustaining battery performance and lifespan [5] and the key to the charger is the charging strategy including the selection of charging current pattern, the control and termination of charging process.

The simple and common charging strategy of a constant current constant voltage (CCCV) is widely used in commercial chargers for lithium-ion batteries [6]. It has two charging stages. In the first constant current (CC) stage, the battery is charged at a constant current until battery terminal voltage reaches a pre-defined value (e.g. 4.2 V). In the second constant voltage (CV) stage, a voltage of the pre-defined value is maintained until the charging current is gradually dropping to the pre-defined value (e.g. 0.05 C), where 0.05 C represents the charging current in C rate which is defined as the ratio of charging current to nominal capacity (C) of a battery. In this study, 0.05 C is chosen as a cut-off current to stop charging process for the CCCV charging method.

Among existing charging methods [7], the multi-stage constant current (MCC) charging method is considered as a high-quality charging pattern with the advantages of long cycle life, high

* Corresponding author. Tel.: +61 3 9214 5886; fax: +61 3 9214 8264.
E-mail addresses: ttvo@swin.edu.au (T.T. Vo), wshen@swin.edu.au (W. Shen).

http://dx.doi.org/10.1016/j.jpowsour.2014.09.108
0378-7753/

charge/discharge energy efficiency and short charging time [8]. Many attempts were proposed to optimise charging current pattern for MCC charging methods. It is regarded as a combinatorial optimisation problem. Such a problem is difficult to be solved by exhaustive search [9]. On one hand, global optimisation techniques, such as genetic algorithm (GA), ant colony system (ACS) and particle swarm optimisation (PSO), were used to search for optimal charging current pattern [10–12]. On the other hand, Taguchi method (TM) was utilised and applied an orthogonal array (OA) to design charging current patterns so that only a small number of experiments were required in order to search optimal charging current pattern [13,14]. For these MCC charging methods, the predefined voltage (e.g. 4.2 V) is used to switch each of the charging stages as well as a cut-off voltage to stop charging process.

In this paper, an optimal charging strategy based on the MCC charging method has been developed with the integration of the TM and the state of charge (SOC) estimation. The TM is applied to search optimal charging current pattern. The estimated SOC is used to control and terminate the charging process. The experimental results of LiPBs have been used to verify the effectiveness of the new charging strategy. The remaining parts of this paper are organised as follows: Section 2 experimentally explores the influences of various charging current levels on charging time, charging efficiency and temperature variation during charging process to assist in selecting charging current candidates to form charging patterns; Section 3 presents a new charging approach. Section 4 shows the experimental results to validate the proposed charging method by comparing it with the equivalent CCCV charging method. Section 5 concludes the paper.

2. Experimental

2.1. Battery testing platform

A battery testing platform has been constructed to conduct the experiments. It consists of a programmable power supply, a programmable electronic load and a safety control switch box. The LabVIEW software program has been used to implement charging strategies by setting different charge currents (or current profiles), sample experimental data and store the data into the computer for further analysis. The details of this platform can be found in Ref. [15].

Turnigy lithium-polymer batteries (LiPBs) with the nominal capacities of 5.8 Ah and 5.0 Ah are used in the experiments, which correspond to the dimensions of 136 mm × 50 mm × 10 mm and 135 mm × 50 mm × 9 mm and the weights of 143 g and 130 g, respectively. These batteries comprise of $LiMn_2O_4$ cathode and an artificial graphite anode. They are usually laminated with the solid electrolyte and the separator sheets, and enclosed in a foil-type case. They have the nominal voltage of 3.7 V with the maximum voltage of 4.2 V for charge and the minimum cut-off voltage of 2.7 V for discharge.

2.2. Testing of a LiPB using CCCV charging method

A LiPB with the nominal capacity of 5.8 Ah (B1) is selected to conduct experiments. The CCCV charging method is adopted to investigate the influences of various charging current levels on charging efficiency, charging time and temperature variation during charging process. According to battery manufacturer's datasheet, it is recommended that the charging current of 0.3 C is for normal charge and the maximum charging current of 2.0 C is for fast charge. Thus, five charging currents of 2.0 C, 1.5 C, 1.0 C, 0.7 C and 0.3 C in the CC stage of the CCCV charging method have been chosen to charge the battery at room temperature, where initially the battery is fully discharged (e.g. SOC = 0%). In the CV stage, the preset voltage of 4.2 V is maintained to charge the battery until the charging current is gradually reduced to 0.05 C, which means that the battery is fully charged (e.g. SOC = 100%). Then, this fully charged LiPB is discharged at the current of 1.0 C until the battery is fully discharged with the cut-off voltage of 2.7 V. For each of these five charging and discharging processes, the experimental data of the currents, voltages and temperatures are collected for analysis. The corresponding results are shown in Fig. 1 and Table 1, respectively. Based on the observation of these experimental results, a few points can be made to help in proposing a new charging strategy which can achieve high energy efficiency, short charging time, and low temperature variation in Section 3.1.1.

- The charging current of 2.0 C is allowed to charge the battery up to almost 90% of nominal capacity in the existing arrangement of the CCCV charging methods. Since 2.0 C is the maximum charging current for the battery, if it is used to charge the battery all the time, the cycle life of the battery will be decreased significantly because lithium plating can be formed at high charging current particularly when the battery is in high SOCs and high temperature [16,17]. Thus, high charging current should be avoided in high SOCs to minimise its effect on battery cycle life and the proposed charging strategy will select the charging current based on the estimated SOC.
- The higher the charging current is, the shorter the charging time, the higher the temperature variation and the lower the energy efficiency are. The highest charging current of 2.0 C results in the lowest energy efficiency, shortest charging time and largest temperature variation while the lowest charging current of 0.3 C results in the highest energy efficiency, longest charging time and lowest temperature variation. Thus, the combination of different levels of charging currents will be adopted in the proposed charging strategy to achieve the balance of energy efficiency, charging time and temperature variation.
- The ampere hour (Ah) efficiencies for all the charging currents are almost 100%, which indicates that this battery can deliver all the ampere hours at 1.0 C no matter what charging currents varying from 0.3 C to 2.0 C are adopted. Thus, the Ah efficiency

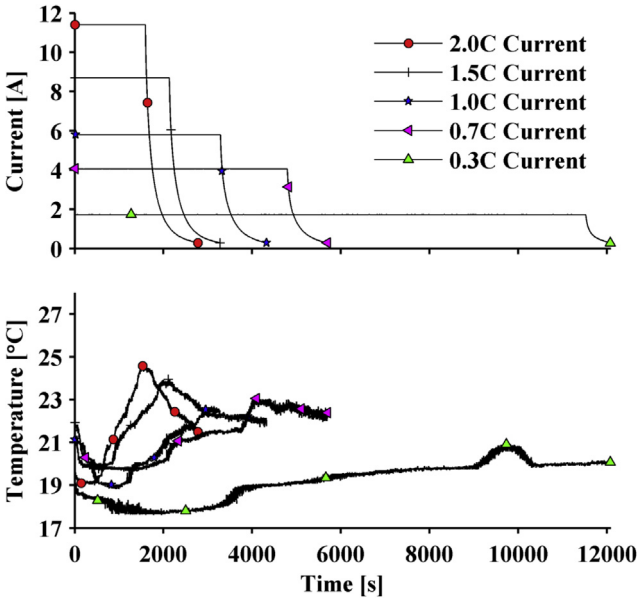

Fig. 1. Experimental results for different charging currents in CC stage of CCCV charging methods.

Table 1
Experimental results of different charging currents in CC stage of CCCV charging method.

Charging current	Charging time	Temperature variation	Ah efficiency	Energy efficiency
2.0 C	2775 s	5.58 °C	100%	96.14%
1.5 C	3271 s	4.31 °C	100%	96.46%
1.0 C	4325 s	3.70 °C	99.95%	96.84%
0.7 C	5691 s	3.40 °C	100%	97.40%
0.3 C	12,078 s	3.31 °C	99.80%	97.51%

will not be considered in the TM to search optimal charging current pattern.

- The influences of charging current levels on energy efficiency, charging time, temperature variation are only appreciable when the charging current differences are 0.5 C (e.g. from 2.0 C, 1.5 C to 1.0 C) and 0.3 C (from 1.0 C, 0.7 C to 0.3 C) from one CCCV charging method to another, respectively. Thus, charging current candidates are not necessary to be chosen as many as those in the existing MCC charging methods with the current difference of 0.05 C [12–14], leading to significant simplification of the searching process for optimal charging current pattern.

2.3. Testing of LiPBs using current pulse charge

As mentioned earlier, the estimated SOC controls and terminates the charging process in the new charging strategy. Thus, it is important to accurately estimate the SOC during the charging process. In this study, a relationship between the open circuit voltage (OCV) and the SOC is used to estimate the SOC. To evaluate the capacity and ageing effect on such a relationship for the same type of batteries, the pulse current charge (PCC) test has been conducted for four LiPBs with the capacities of 5.8 Ah (B1 and B2) and 5.0 Ah (B3 and B4), respectively, where B1 and B2 have different numbers of cycles and so are B3 and B4. The procedure of conducting the PCC test is explained as follows. Initially, four LiPBs are fully discharged (SOC = 0%) and left in the open circuit state for an hour so that the OCV is able to reach its equilibrium state at room temperature. Then, they are charged by a sequence of 1.0 C pulse current consisting of six minutes charge equivalent to 10% of the SOC increment and one hour rest until the charge current reaches the cut-off current of 0.05 C when the batteries are considered to be fully charged (SOC = 100%). The experimental results of these four batteries are illustrated in Fig. 2. It can be seen that the relationship between the OCV and the SOC for these four batteries are almost the same, which shows that the SOC estimation can be used to control the charging process for these types of LiPBs regardless of their capacities and cycle life.

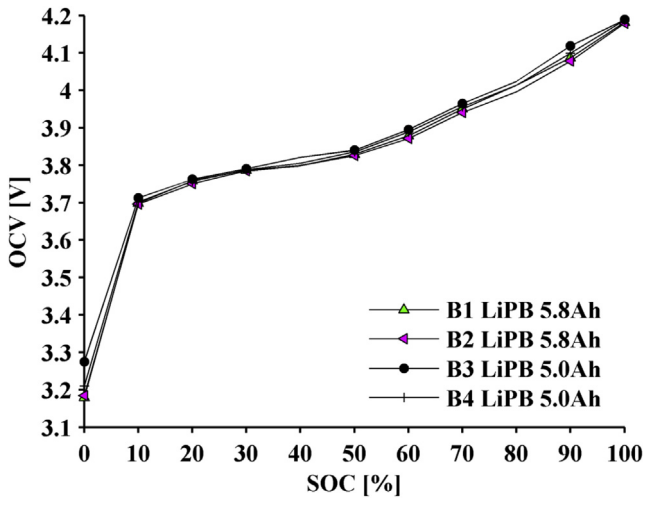

Fig. 2. Experimental results for relationship of OCV versus SOC for LiPBs.

3. Proposed charging strategy

3.1. Taguchi-based optimal charging pattern searching algorithm

The TM was initially developed by Genichi Taguchi for optimising manufacturing process and then accommodated into the fields such as mechanical engineering, power electronics, and radio networks [18–21]. For the optimisation problems with all possible combinations of parameters, the TM is suitable for finding the optimal parameters and decreasing the number of necessary experiments.

3.1.1. Charging current pattern formulation

According to the discussions in Section 2.2, a four-stage constant current (FSCC) charging method is proposed in this paper and conceptually shown in Fig. 3. The total charging period is equally divided into four stages, where each stage has the range of the SOC equal to 25%. In each stage, the LiPB is charged by a pre-set current. During charging process, the SOC is estimated. When the estimated SOC reaches the predetermined SOC, the charging process will be shifted to next stage and a new pre-set charging current will be applied accordingly. The charging process will continue until the estimated SOC reaches 100% when the battery is fully charged and the charging process terminates.

In the proposed FSCC charging method, the combination of different levels of charging current in four stages will lead to different charging current patterns. Table 2 shows the charging current candidates in this study where the charging current in each stage has three different levels with the current difference of 0.1 C, the charging current in different stages has the current difference of 0.5 C and the charging currents at the present stage are lower than those of previous stage. From Table 2, the number of a full factorial charging pattern requires 81 experiments. In each experiment, a specific charging current pattern charges the fully discharged battery to determine the charging time and the temperature variation over the charging process and then the battery is discharged at a predefined constant current of 1.0 C to evaluate the influence of each charging current pattern on energy efficiency. Obviously, it is not wise to test all 81 possible charging current patterns to search

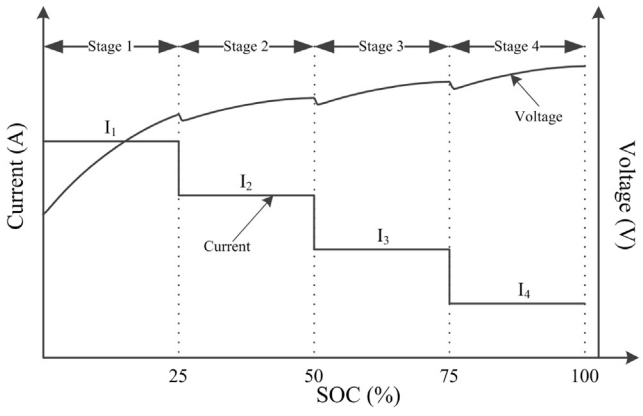

Fig. 3. Proposed charging current pattern.

Table 2
Charging current candidates for four charging stages.

Stage name	High	Medium	Low
Stage S_1	2.0 C	1.9 C	1.8 C
Stage S_2	1.5 C	1.4 C	1.3 C
Stage S_3	1.0 C	0.9 C	0.8 C
Stage S_4	0.5 C	0.4 C	0.3 C

the optimal one. To eliminate the lengthy experimental procedure while taking advantage of the performance of a full factorial experimental design, the TM is developed to search in the parameter space with a small number of experiments based on the orthogonal arrays (OAs) technique. According to the most commonly used standard OAs for experimental design [14], the search of an optimal charging current pattern can be performed among only 9 patterns represented by $L_9(3^4)$, where 3 and 4 are the number of charging current levels in each stage and the number of stages in each charging current pattern shown in Table 2, respectively. These 9 charging current patterns as shown in Table 3 correspond to 9 experiments. With these patterns selected on the basis of the TM method, the interactions between the current levels are quasi-uniformly distributed between the columns of Table 3 and are nearly independent [22]. In Table 3, the High, Medium and Low represent different levels of charging current for each stage, respectively. For example, the charging current pattern of High, High, High and High in experiment no. 1 stands for the FSCC charging pattern with the charging current sequences of 2.0 C, 1.5 C, 1.0 C, 0.5 C. Once each experiment is completed, the experimental results are considered as the responses y_{ij} with $i = 1, 2, \ldots, 9$ which is the number of the experiment and $j = 1, 2, 3$ which is corresponding to energy efficiency, charging time and temperature variation, respectively.

The experiments of 9 charging current patterns are conducted on 5.8 Ah LiPB (B1) at room temperature. During the charging process, the SOC estimation is carried out (see the detailed explanation of the SOC estimation in Section 3.2). When the estimated SOC reaches to 25%, 50% and 75%, respectively, the charging process will switch to the next stage. When the estimated SOC reaches to 100%, the charging process terminates. Once the charging process is completed, the battery is discharged at the constant current of 1.0 C until the battery voltage reaches to the cut-off voltage of 2.7 V. During charging/discharging processes, if the battery temperature is higher than 45 °C, the process also terminates to protect the battery from thermal runaway. The energy efficiency over the charging process is calculated, and the charging time and temperature variation are collected. All responses from the experimental results are shown in Table 4. For example, the experiment no. 9 ($i = 9$) has three responses: energy efficiency ($j = 1$) of 95.96%, charging time ($j = 2$) of 3618 s and temperature variation ($j = 3$) of 1.78 °C.

Table 3
All 9 charging current patterns based on $L_9(3^4)$ orthogonal array.

Exp. no.	Stage 1	Stage 2	Stage 3	Stage 4	Responses ($j = 1, 2, 3$)
1	High	High	High	High	y_{1j}
2	High	Medium	Medium	Medium	y_{2j}
3	High	Low	Low	Low	y_{3j}
4	Medium	High	Medium	Low	y_{4j}
5	Medium	Medium	Low	High	y_{5j}
6	Medium	Low	High	Medium	y_{6j}
7	Low	High	Low	Medium	y_{7j}
8	Low	Medium	High	Low	y_{8j}
9	Low	Low	Medium	High	y_{9j}

Table 4
Responses (experimental results) for energy efficiency, charging time and temperature variation.

Exp. No. (i)	Responses (y_{ij})		
	Energy eff. (%) for $j = 1$	Charging time (s) for $j = 2$	Temp. var. (°C) for $j = 3$
1	95.53	3313	4.97
2	95.12	3939	3.60
3	95.30	4826	2.99
4	95.11	4571	4.22
5	95.15	3599	2.97
6	95.11	3932	2.73
7	95.99	4070	3.95
8	95.68	4602	2.17
9	95.96	3618	1.78

3.1.2. Searching optimal charging current pattern

The purpose of the new charging strategy is to improve charging efficiency, reduce charging time and narrow down temperature variation in the comparison of CCCV charging methods. To achieve this by using the TM, the experimental results shown in Table 4 are divided into two types: the larger-the-better (LTB) for energy efficiency and the smaller-the-better (STB) for both charging time and temperature variation. The TM employs signal to noise (S/N) ratio as a quality measurement. For each type of response ($j = 1$, 2 or 3), the optimal factor level is the factor level which maximises S/N ratio, β_{ij}.

$$\beta_{ij} = \begin{cases} -10\log_{10}\left(\frac{1}{n}\sum_{k=1}^{n}\frac{1}{\left(y_{ij.k}\right)^2}\right), & \text{For LTB type response} \\ -10\log_{10}\left(\frac{1}{n}\sum_{k=1}^{n}\left(y_{ij,k}\right)^2\right), & \text{For STB type response} \end{cases} \quad (1)$$

where n is the number of replicates for $y_{ij,k}$, where $k = 1,2,3, \ldots, n$.

In order to solve multi-responses problem in the TM, the following steps are utilised [23]:

Step 1: The S/N ratios (β_{ij}) for energy efficiency (LTB type), charging time and temperature variation (STB type) are calculated from the responses (experimental results) from Table 4 using Eq. (1) and shown in Table 5.

Step 2: The average S/N ratios, $\overline{\beta}_{j,m,n}$, for three types of responses (1 stands for energy efficiency, 2 for charging time, 3 for temperature variation) with three levels (n = charging current levels: High, Medium, Low) of four factors (m = charging stages: S1, S2, S3 and S4) are estimated from responses (β_{ij}) in Table 5.

Table 5
S/N ratios for energy efficiency, charging time and temperature variation.

Exp. No. (i)	Responses (β_{ij})		
	Energy eff. (dB) for $j = 1$	Charging time (dB) for $j = 2$	Temp. var. (dB) for $j = 3$
1	39.603	−70.404	−13.925
2	39.565	−71.908	−11.118
3	39.582	−73.672	−9.516
4	39.565	−73.200	−12.505
5	39.568	−71.124	−9.448
6	39.565	−71.892	−8.732
7	39.645	−72.192	−11.926
8	39.616	−73.259	−6.740
9	39.642	−71.169	−5.023

To illustrate the calculation of $\overline{\beta}_{j,m,n}$, assume that $\overline{\beta}_{1,S_1,\text{High}}$ represents the average S/N ratio for $S_{1,\text{High}}$; it is an average of the S/N ratios for the experiment no. 1, 2, and 3 for energy efficiency, namely $\overline{\beta}_{1,S_1,\text{High}} = \frac{1}{3}(\beta_{11} + \beta_{21} + \beta_{31}) = 39.583$ dB, and $\overline{\beta}_{1,S_1,\text{Medium}}$(39.566 dB) and $\overline{\beta}_{1,S_1,\text{Low}}$(39.634 dB) are the average of the S/N ratios of experiment no. 4, 5, 6 and experiment no. 7, 8, 9, respectively. In the same way $\overline{\beta}_{j,S_1,\text{High}}$, $\overline{\beta}_{j,S_1,\text{Medium}}$ and $\overline{\beta}_{j,S_1,\text{Low}}$ are calculated for $j = 2$ and 3, and the average S/N ratios for the stages 2–4 can also be calculated from each response β_{ij}. As a result, all the average S/N ratios are shown in Table 6. The TM in Refs. [24,25] is utilised to select the main effects for each charging stage. According to Table 6, the optimal factor levels with the number highlighted in bold are $S_{1,\text{Low}}$, $S_{2,\text{High}}$, $S_{3,\text{Low}}$, $S_{4,\text{High}}$; for energy efficiency, $S_{1,\text{High}}$, $S_{2,\text{High}}$, $S_{3,\text{High}}$, $S_{4,\text{High}}$ for charging time and $S_{1,\text{Low}}$, $S_{2,\text{Low}}$, $S_{3,\text{Medium}}$, $S_{4,\text{High}}$ for temperature variation. The optimal charging pattern is the balance of these main effects and decided by using average level weight in next step.

Step 3: Let $\omega_{j,m,n}$ be the weight of level n for factor m from response $\overline{\beta}_{j,m,n}$, which is calculated as

$$\omega_{j,m,n} = \begin{cases} \dfrac{\overline{\beta}_{j,m,n}}{\max_n \overline{\beta}_{j,m,n}}, & \text{For LTB type response} \\ \dfrac{\max_n \overline{\beta}_{j,m,n}}{\overline{\beta}_{j,m,n}}, & \text{For STB type response} \end{cases} \quad (2)$$

According to Eq. (2), $\omega_{1,S_1,\text{High}}$,$\omega_{1,S_1,\text{Medium}}$ and $\omega_{1,S_1,\text{Low}}$ of 3 levels of S1 are calculated for energy efficiency ($j = 1$) as 0.9987(=39.583/39.634), 0.9983(=39.566/39.634), 1.0000(=39.634/39.634), and $\omega_{j,S_1,\text{High}}$,$\omega_{j,S_1,\text{Medium}}$,$\omega_{j,S_1,\text{Low}}$ can also be calculated for charging time ($j = 2$) and temperature variation ($j = 3$), respectively. Similarly, the calculations of all $\omega_{j,m,n}$ can be made for stages 2–4, they are all shown in Table 7. Let $\overline{W}_{m,n}$ be the average of $\omega_{j,m,n}$ over all responses at the same level (n) and factor (m), then $\overline{W}_{S_1,\text{High}}$, $\overline{W}_{S_1,\text{Medium}}$, $\overline{W}_{S_1,\text{Low}}$ are calculated from three responses in the S1 as 0.8947, 0.9231, 0.9990, respectively. Since the maximum level weight for S1 corresponds to $S_{1,\text{Low}}$, the optimal level of S1 is decided as Low. Similarly, $\overline{W}_{m,n}$ values are calculated for S2, S3 and S4, where their optimal values are Low, Medium, and High, respectively. Therefore, the optimal charging current pattern is the sequence of 1.8 C, 1.3 C, 0.9 C and 0.5 C.

3.2. Online SOC estimation

Online SOC estimation is used to control the change of the charging stage and terminate charging process without overcharging LiPBs. An adaptive switching gain sliding mode observer (ASGSMO) based on battery equivalent circuit model (BECM) is adopted in this paper for the SOC estimation [15,26].

Table 6
Average S/N ratios for energy efficiency, charging time and temperature variation.

Responses (dB)	Factor (m)	Stage S_1	Stage S_2	Stage S_3	Stage S_4
	Level (n)				
Energy eff.	High	39.583	**39.604**	39.595	**39.604**
	Medium	39.566	39.583	39.591	39.591
	Low	**39.634**	39.596	**39.598**	39.588
Charging time	High	**−71.995**	**−71.932**	**−71.852**	**−70.899**
	Medium	−72.072	−72.097	−72.092	−71.997
	Low	−72.207	−72.245	−72.329	−73.377
Temp. var.	High	−11.520	−12.785	−9.799	**−9.465**
	Medium	−10.228	−9.102	**−9.549**	−10.592
	Low	**−7.896**	**−7.757**	−10.297	−9.587

The bold number indicates the biggest number in each stage, the level corresponding to that number has the largest effects.

Table 7
Level weights for energy efficiency, charging time and temperature variation.

Response (dB)	Factor (m)	Stage S_1	Stage S_2	Stage S_3	Stage S_4
	Level (n)				
Energy eff.	High	0.9987	1.0000	0.9999	1.0000
	Medium	0.9983	0.9995	0.9998	0.9997
	Low	1.0000	0.9998	1.0000	0.9996
Charging time	High	1.0000	1.0000	1.0000	1.0000
	Medium	0.9989	0.9977	0.9967	0.9847
	Low	0.9971	0.9957	0.9934	0.9662
Temp. var.	High	0.6854	0.6067	0.9745	1.0000
	Medium	0.7720	0.8522	1.0000	0.8936
	Low	1.0000	1.0000	0.9274	0.9873
Level weight	High	0.8947	0.8689	0.9915	**1.0000**
	Medium	0.9231	0.9498	**0.9988**	0.9593
	Low	**0.9990**	**0.9985**	0.9736	0.9844

The bold number indicates the selection of level of charging current for each stage.

3.2.1. Adaptive switching gain sliding mode observer for SOC estimation

A variety of battery models has been developed to capture dynamic characteristics of LiPBs for achieving accurate estimation of battery states [27–29]. A BECM consisting of lumped circuit components such as capacitors, resistors, voltage sources is utilised in this paper. The schematic diagram of the BECM is shown in Fig. 4, where the variations of the circuit parameters are included to represent the modelling errors.

In the BECM, a capacitor C_n as the nominal capacity represents the total stored energy in the battery. The current source, I denotes the charge or discharge current of the LiPB and V_t expresses the corresponding battery terminal voltage. The voltage across the C_n as the OCV, V_{oc} varies in the range of the SOC, Z from 0% to 100% and it represents the SOC quantitatively. An ohmic resistor R_{in} characterises the charging energy losses of battery. Two parallel resistive and capacitive networks comprise of the electrochemical polarisation resistance R_{pe}, capacitance C_{pe}, the concentration polarisation resistance R_{pc} and capacitance C_{pc}, which reflect the short-term and long-term transient responses due to the relaxation effect of battery, respectively. This relaxation effect represents the slow convergence of battery terminal voltage to the OCV at its equilibrium state. The voltage-controlled voltage source, V_{oc} (Z) is used to bridge the nonlinear relationship between the SOC and the OCV as shown in Fig. 2. The self-discharge resistance is ignored in this model as the LiPB has extremely low self-discharge rate. The symbols ΔV_{oc}, ΔR_{in}, ΔR_{pe}, ΔC_{pe}, ΔR_{pc} and ΔC_{pc} reflect variations of the circuit parameters caused by the adoption of the constant values of the BECM parameters and the piecewisely linearised relationship of OCV-SOC curves.

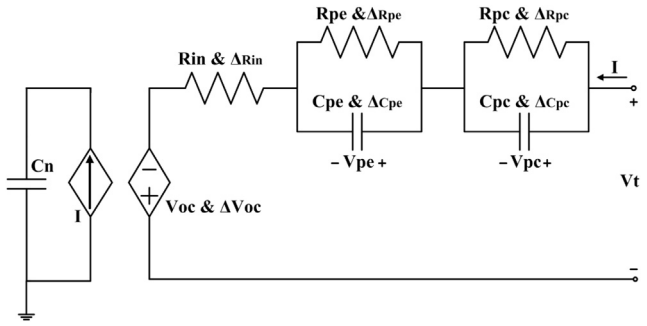

Fig. 4. Schematic of battery equivalent circuit model.

The SOC indicates the ratio of charged capacity to the nominal capacity, and it is expressed as.

$$Z(t) = Z(0) + (1/C_n)\int_0^t \eta I(\tau)\mathrm{d}\tau \tag{3}$$

where $Z(0)$ denotes the initial SOC, C_n is the battery nominal capacity in Ah, $I(\tau)$ is the instantaneous charge current (assumed to be positive), and η is Ah efficiency, which is close to 100% for LiPBs in the wide range of current and temperature as shown in Table 1.

According to Kirchhoff voltage law in circuit theory, the battery terminal voltage V_t can be expressed as.

$$V_t = V_{oc}(Z) + V_{pe} + V_{pc} + IR_{in} + \Delta_{uncertain} \tag{4}$$

The time derivatives of the SOC and polarisation voltages yield.

$$\dot{Z} = (I/C_n) + \Delta f_2 \tag{5}$$

$$\dot{V}_{pe} = -V_{pe}/(R_{pe}C_{pe}) + I/C_{pe} + \Delta f_3 \tag{6}$$

$$\dot{V}_{pc} = -V_{pc}/(R_{pc}C_{pc}) + I/C_{pc} + \Delta f_4 \tag{7}$$

where V_{pe} and V_{pc} denote the electrochemical and concentration polarisation voltages across C_{pe} and C_{pc}, respectively. The terms $\Delta_{uncertain}$, Δf_2, Δf_3 and Δf_4 represent model uncertainties and time-varying internal and external disturbances.

Despite the nonlinearity of OCV-SOC curves as shown in Fig. 2, there exists a piecewise linear relationship between the OCV and the SOC in a certain range of the SOC. Thus, the OCV can be expressed as a function of the SOC by using piecewise linearisation method.

$$V_{oc}(Z) = \kappa Z + \nu \tag{8}$$

where the linearised coefficients of κ and ν are varying in different SOC ranges.

Due to the fast sampling rate and constant charging current rates in each stage, the time derivative of charging current can be negligible, namely $\mathrm{d}I/\mathrm{d}t = 0$, and thereby the time derivative of terminal voltage V_t in Eq. (4) with the substitutions of Eqs. (5)–(7) gives.

$$\dot{V}_t = \kappa(I/C_n) - V_{pe}/(R_{pe}C_{pe}) + I/C_{pe} - V_{pc}/(R_{pc}C_{pc}) + I/C_{pc} + \Delta f_1 \tag{9}$$

Solving I in Eq. (4) and substituting it into Eq. (5) as well as rearranging Eqs. (6)–(8) yield the state-space equations of the BECM as follows.

$$\begin{aligned}
\dot{V}_t &= -a_1 V_t + a_1 V_{oc}(Z) + a_3 V_{pe} + a_4 V_{pc} + b_1 I + \Delta f_1 \\
\dot{Z} &= a_2 V_t - a_2 V_{oc}(Z) - a_2 V_{pe} - a_2 V_{pc} + \Delta f_2 \\
\dot{V}_{pe} &= -a_4 V_{pe} + b_2 I + \Delta f_3 \\
\dot{V}_{pc} &= -a_3 V_{pc} + b_3 I + \Delta f_4
\end{aligned} \tag{10}$$

where $a_1 = 1/(R_{pe}C_{pe}) + 1/(R_{pc}C_{pc})$, $a_2 = 1/(R_{in}C_n)$, $a_3 = 1/(R_{pc}C_{pc})$, $a_4 = 1/(R_{pe}C_{pe})$, $b_1 = \kappa/C_n + R_{in}/(R_{pe}C_{pe}) + 1/C_{pe} + R_{in}/(R_{pc}C_{pc}) + 1/C_{pc}$, $b_2 = 1/C_{pe}$ and $b_3 = 1/C_{pc}$.

If the input and the output of circuit model are defined as $u(t) = I$ and $y(t) = V_t$, respectively, and the system state variables are chosen as V_t, V_{oc}, V_{pe} and V_{pc}, then Eq. (10) can be concisely expressed in matrices.

$$\dot{x}(t) = Ax(t) + Bu(t) + \Delta f(x,u,t) \tag{11}$$

$$y(t) = Cx(t) \tag{12}$$

where

$$A = \begin{bmatrix} -a_1 & a_1 & -a_3 & -a_4 \\ a_2 & -a_2 & a_2 & a_2 \\ 0 & 0 & -a_4 & 0 \\ 0 & 0 & 0 & -a_3 \end{bmatrix}, B = \begin{bmatrix} -b_1 \\ 0 \\ b_2 \\ b_3 \end{bmatrix}, C = [1 \quad 0 \quad 0 \quad 0]$$

and $x(t) = [V_t \quad Z \quad V_{pe} \quad V_{pc}]^T$

The unknown function $\Delta f(x,u,t)$ represents the matched model uncertainties and it can be assumed that.

$$\Delta f(x,u,t) = \Gamma\xi(x,t) \tag{13}$$

where Γ is the model uncertainties input matrix and the function $\xi(x,t)$ is unknown but bounded

$$|\xi(x,t)| \le \psi \quad \forall x \in R^4, \ t \ge 0 \tag{14}$$

where the bound ψ is a positive constant and can be determined by the largest modelling errors between the experimental data and the BECM of the LiPBs. Substituting Eq. (13) into Eq. (11) gives

$$\dot{x}(t) = Ax(t) + Bu(t) + \Gamma\xi(x,t) \tag{15}$$

According to [25], the ASGSMO for the SOC estimation of LiPBs is derived as follows.

$$\dot{\hat{x}}(t) = A\hat{x}(t) + Bu(t) + K(y(t) - C\hat{x}(t)) + \upsilon \tag{16}$$

$$\hat{y}(t) = C\hat{x}(t) \tag{17}$$

where the feedback gain matrix, K and the adaptive switching gains function, υ can be designed so that the stability and robustness of the ASGSMO is ensured.

$$\upsilon = \begin{cases} \hat{\theta}(e_y(t))\Gamma\mathrm{sgn}(e_y(t)) & \text{if } e_y(t) \ne 0 \\ 0 \quad \text{otherwise} \end{cases} \tag{18}$$

The discontinuous switching term is defined as.

$$\mathrm{sgn}(e_y(t)) = \begin{cases} +1, & e_y(t) > 0 \\ -1, & e_y(t) < 0 \end{cases} \tag{19}$$

where $e_y(t) = y(t) - \hat{y}(t) = Ce(t)$ and the adaptive switching gain $\hat{\theta}(Ce(t))$ is updated by the following adaptive law

$$\dot{\hat{\theta}}(e_y(t)) = \alpha|e_y(t)| \tag{20}$$

where α is a positive constant, which can be chosen to adjust the speed adaptation for switching gains function. As the switching gains are updated correspondingly to the state error dynamics, the ASGSMO can provide robust tracking capability against modelling errors while significantly reducing the magnitude of chattering in the SOC estimation.

3.2.2. Battery equivalent circuit model parameters identification

The parameters of the BECM shown in Fig. 4 are extracted from the least square estimation method by executing a PCC profile as a battery characterisation test at room temperature. As an example, the PCC profile is performed to identify the BECM parameters of

5.8 Ah LiPB (B1). The corresponding current and voltage response is shown in Fig. 5. It can be seen that there are totally ten sets of transient responses as the battery terminal voltage converged to its associated OCV after one hour relaxation.

From Eq. (4), the voltage difference between terminal voltage and the OCV can be defined as $V_d = (V_t - V_{oc})$ such that.

$$V_d = V_{pe} + V_{pc} + IR_{in} \tag{21}$$

Based on Eqs. (6), (7) and (21), the system transfer function of the BECM can be derived as follows.

$$V_d(s) = \left(\frac{R_{pe}}{1 + sR_{pe}C_{pe}} + \frac{R_{pc}}{1 + sR_{pc}C_{pc}} + R_{in}\right) I(s) \tag{22}$$

It can be transformed into the difference equation form.

$$\begin{aligned} &V_t(k+2) + \theta_1 V_t(k+1) + \theta_2 V_t(k) \\ &\quad = \theta_3 I(k+2) + \theta_4 I(k+1) + \theta_5 I(k) + \theta_6 \end{aligned} \tag{23}$$

where k denotes the time step and $\theta_1 = 1/(R_{pe}C_{pe}) + 1/(R_{pc}C_{pc})$, $\theta_2 = 1/(R_{pe}C_{pe}R_{pc}C_{pc})$, $\theta_3 = R_{in}$, $\theta_4 = (R_{in} + R_{pe})/(R_{pe}C_{pe}) + (R_{in} + R_{pc})/(R_{pc}C_{pc})$, $\theta_5 = (R_{in} + R_{pe} + R_{pc})/(R_{pe}R_{pc}C_{pe}C_{pc})$ and $\theta_6 = V_{oc}$, and the BECM parameters will be estimated based on coefficients of Eq. (23).

There exist n sets of sampled data, as shown in the following matrix form.

$$\begin{bmatrix} V_t(k+2) \\ V_t(k+3) \\ \vdots \\ V_t(n) \end{bmatrix} = \begin{bmatrix} -V_t(k+1) & -V_t(k) & I(k+2) & I(k+1) & I(k) & 1 \\ -V_t(k+2) & V_t(k+1) & I(k+3) & I(k+2) & I(k+1) & 1 \\ \vdots & \vdots & \vdots & \vdots & \vdots & \vdots \\ -V_t(n-2) & -V_t(n-1) & I(n) & I(n-1) & I(n-2) & 1 \end{bmatrix} \cdot \begin{bmatrix} \theta_1 \\ \theta_2 \\ \theta_3 \\ \theta_4 \\ \theta_5 \\ \theta_6 \end{bmatrix} \tag{24}$$

Eq. (24) can be further concisely expressed in following form.

$$U = \Phi \cdot \Theta \tag{25}$$

where $U = [\,V_t(k+2) \quad V_t(k+3) \quad \cdots \quad V_t(n)\,]^T$,

$$\Phi = \begin{bmatrix} -V_t(k+1) & -V_t(k) & I(k+2) & I(k+1) & I(k) & 1 \\ -V_t(k+2) & V_t(k+1) & I(k+3) & I(k+2) & I(k+1) & 1 \\ \vdots & \vdots & \vdots & \vdots & \vdots & \vdots \\ -V_t(n-2) & -V_t(n-1) & I(n) & I(n-1) & I(n-2) & 1 \end{bmatrix}$$

and $\Theta = [\,\theta_1 \quad \theta_2 \quad \theta_3 \quad \theta_4 \quad \theta_5 \quad \theta_6\,]^T$ where $[\,]^T$ denotes the transposition of a matrix. Therefore, the least square method can be applied to estimate the parameters based on the following calculation

$$\Theta = \left(\Phi^T \cdot \Phi\right)^{-1} \cdot \Phi^T \cdot U \tag{26}$$

where $()^{-1}$ denotes the inverse of a matrix. Using Eq. (26), the parameters of the BECM for the 5.8 Ah LiPB (B1) are $R_{in} = 3.15$ mΩ, $R_{pe} = 1.651$ mΩ, $R_{pc} = 2.35$ mΩ, $C_{pe} = 1.7896$ kF and $C_{pc} = 5.7368$ kF.

To verify the accuracy of the BECM with the identified parameters, the PCC profile is reloaded into the BECM. Fig. 6 illustrates the comparison of the terminal voltages obtained from the experiment

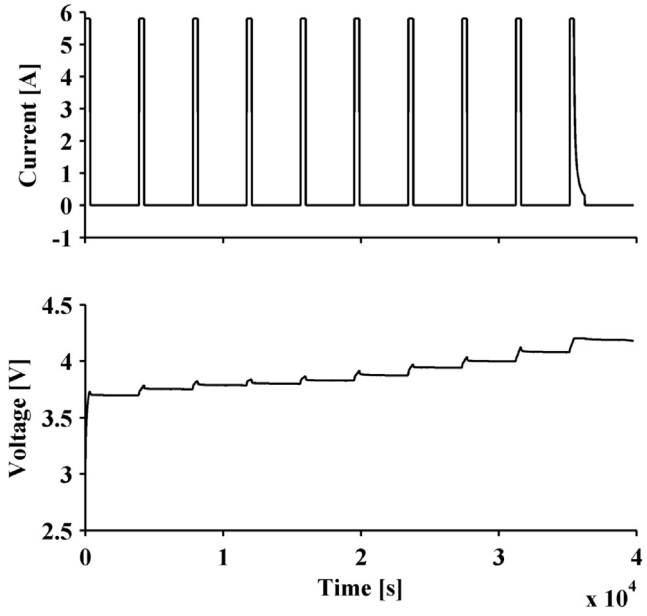

Fig. 5. Pulse current charge and terminal voltages for LiPB B1.

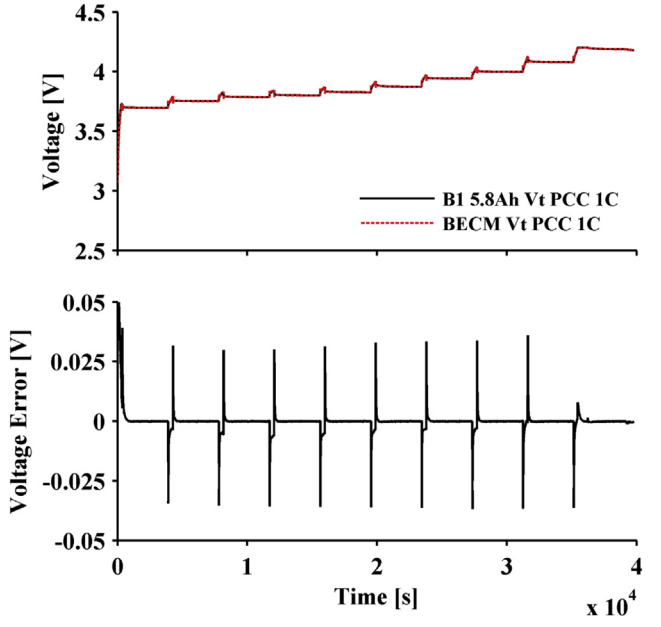

Fig. 6. Comparison of terminal voltage between experimental results of LiPB B1 and those calculated from BECM at PCC with their absolute errors.

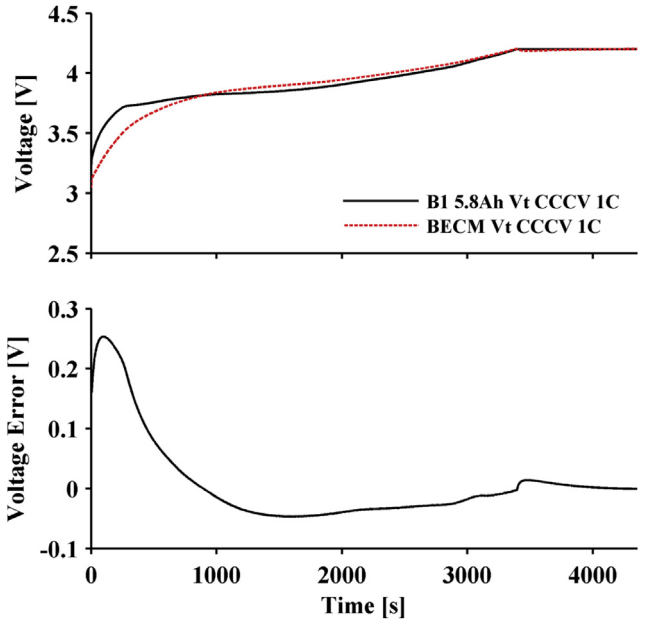

Fig. 7. Comparison of terminal voltage between experimental results of LiPB B1 and those calculated from BECM at CCCV with their absolute errors.

of the 5.8 Ah LiPB (B1) and those calculated from the BECM as well as the associated modelling errors. It shows that the errors are within a small range of −0.025 V~ + 0.025 V. Although the battery terminal voltage of the BECM has a small deviation from those of a real LiPB in the PCC profile, there exist considerable modelling errors for other charging current profiles when the predetermined constant model parameters are used. For example, Fig. 7 shows the comparison of the terminal voltage obtained from the experiment of the 5.8 Ah LiPB (B1) and those calculated from the BECM for the CCCV charging profile with 1.0 C charging current. Nevertheless, the ASGSMO for the SOC estimation can overcome the inaccuracy of the BECM with the constant model parameters and track the SOC accurately.

3.2.3. *Verification of ASGSMO for SOC estimation*

To verify the effectiveness and accuracy of the ASGSMO for the SOC estimation, two charging current profiles have been loaded to the 5.8 Ah LiPB (B1) at the room temperature and these two current profiles are simultaneously applied to the LiPB integrated with Ah counting module and the ASGSMO module as shown in Fig. 8. The LiPB terminal voltage is sampled and fed into the ASGSMO to generate the output tracking error, which can be used to update the corresponding switching gains of ASGSMO for the compensation of the modelling errors. The resultant output of the ASGSMO module is the estimated SOC, which is concurrently compared to the true SOC directly generated by the Ah counting module to show the accuracy of the SOC estimation. The feedback gain matrix, K is obtained by using the LQR method with Riccati equation as $K = [1.6872 \quad 2.7983 \quad 0.8271 \quad 0.3754]^T$ and the model uncertainties input matrix, Γ is defined as $\Gamma = [1.4516 \quad -0.0326 \quad 0.0122 \quad 0.0204]^T$. The positive constant, α is selected as 0.4 to satisfy the adaptation speed for the switching gains function.

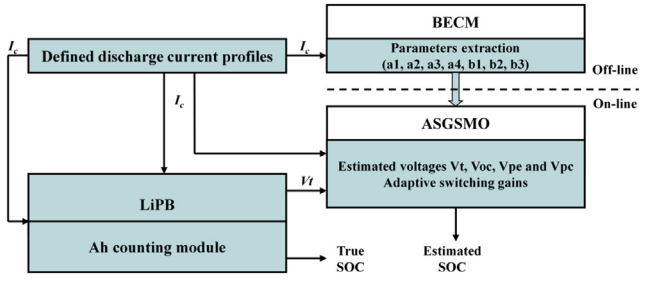

Fig. 8. Verification of ASGSMO for SOC estimation.

The first charging profile is the PCC and its corresponding results of the SOC estimation from charging current of 1.0 C in each pulse charge are shown in Fig. 9. It can be seen that during the one hour resting phase as the true SOC remains same, and the ASGSMO is able to track the true SOC with no chattering ripples, also its SOC estimation errors expressed as the root mean square errors (RMSEs) are limited to the small range of −4% to +2%. This is due to the fact that the switching gains of the ASGSMO can be adaptively tuned to the proper low levels as the corresponding estimation errors decrease.

To further evaluate the ASGSMO for the SOC estimation, another estimation results as shown in Fig. 10 are collected from the CCCV profile with the charging current of 1.0 C. It can be found that in the presence of modelling errors caused by constant model parameters, the ASGSMO is capable of tracking true SOC with the RMSEs in range of −3% to +3%. The estimated SOC is rapidly increasing at the CC stage and it becomes slow increment at the CV stage as the contant battery terminal voltage leads to the quick drop in charging current.

4. Results and discussions

The experiments have been conducted to verify the effectiveness of the new charging strategy, which has the charging current sequence of 1.8 C, 1.3 C, 0.9 C and 0.5 C and is used to charge LiPB 5.8 Ah (B1) with different initial SOCs and the other three LiPBs (B2, B3, and B4) with the same initial SOC. Furthermore, the new charging strategy compares with the equivalent CCCV charging method. The followings are the experimental results and the corresponding discussions.

4.1. *Testing results on LiPB 5.8 Ah (B1) with different initial SOCs*

The new charging strategy has been used to charge LiPB 5.8 Ah (B1) at different initial SOCs. The procedure to conduct the experiments is

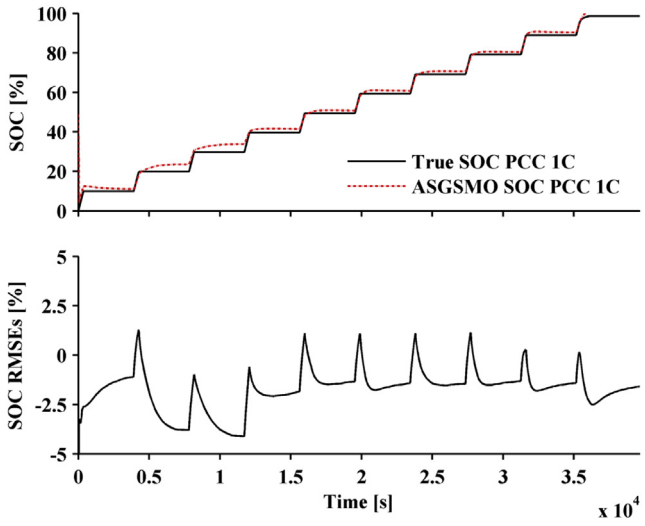

Fig. 9. ASGSMO estimated SOC at PCC with RMSE(%).

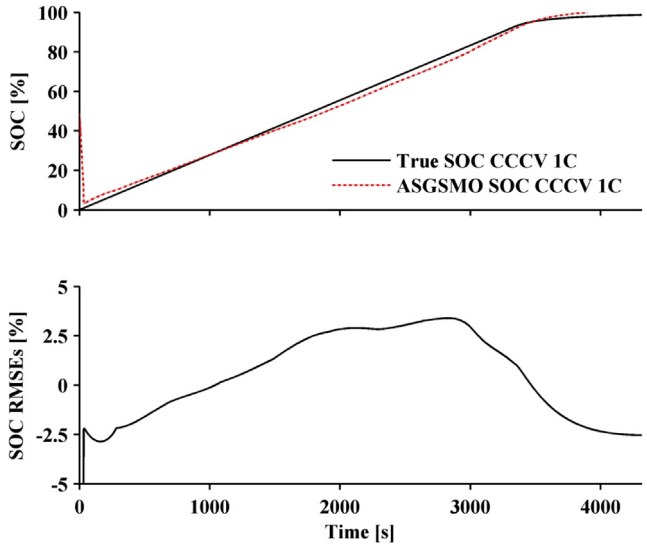

Fig. 10. ASGSMO estimated SOC at CCCV with RMSE(%).

explained as follows. For SOC = 0%, the battery is fully discharged and rested for an hour, and then charged by the new charging strategy. For the other SOCs, the battery is fully discharged and rested for an hour, and then charged by the constant current of 1.0 C to the preset SOCs, such as 17%, 37%, 67% and 84% which are in the ranges of 0%–25%, 25%–50%, 50%–75% and 75%–100%, respectively, and then charged by the new charging strategy. Fig. 11 shows the charging current patterns and the corresponding terminal voltages. It indicates that the new charging strategy can successfully charge the LiPB at any initial SOCs with the assistant of the ASGSMO for the SOC estimation which is used to control and terminate the charging process.

4.2. Testing results on LiPBs 5.8 Ah (B2), 5.0 Ah (B3 and B4) at the same initial SOC

The new charging method has also been used to charge the other three LiPBs 5.8 Ah (B2), 5.0 Ah (B3 and B4). To make

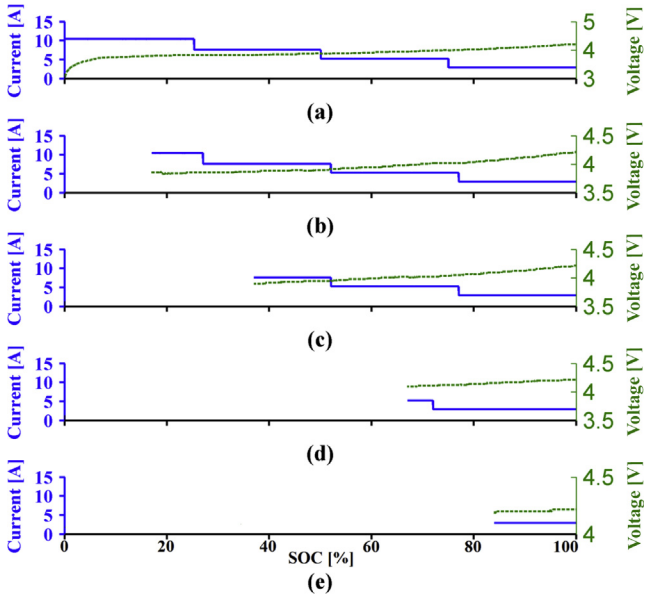

Fig. 11. Experimental results of new charging strategy with different SOCs of LiPB B1 (a) SOC = 0%, (b) SOC = 17%, (c) SOC = 37%, (d) SOC = 67%, (e) SOC = 84%.

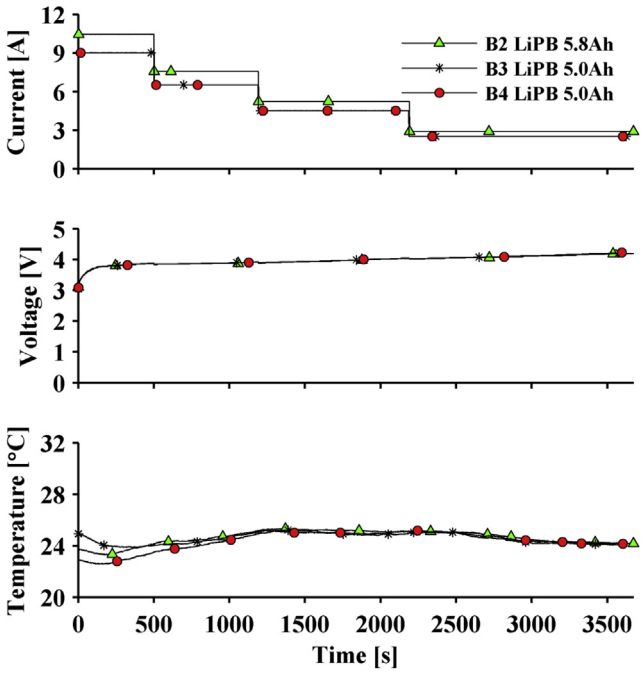

Fig. 12. Experimental results of new charging strategy at SOC = 0% with different LiPBs: B2 (5.8 Ah), B3 (5.0 Ah) and B4 (5.0 Ah).

experimental results understand easily, the initial SOCs for these batteries are set to 0%. Fig. 12 shows the charging current pattern, terminal voltage and temperature variation, their voltage and temperature profiles are quite consistent for these three batteries. It shows that the new charging strategy can apply to the same type of LiPBs with different capacities and cycle life.

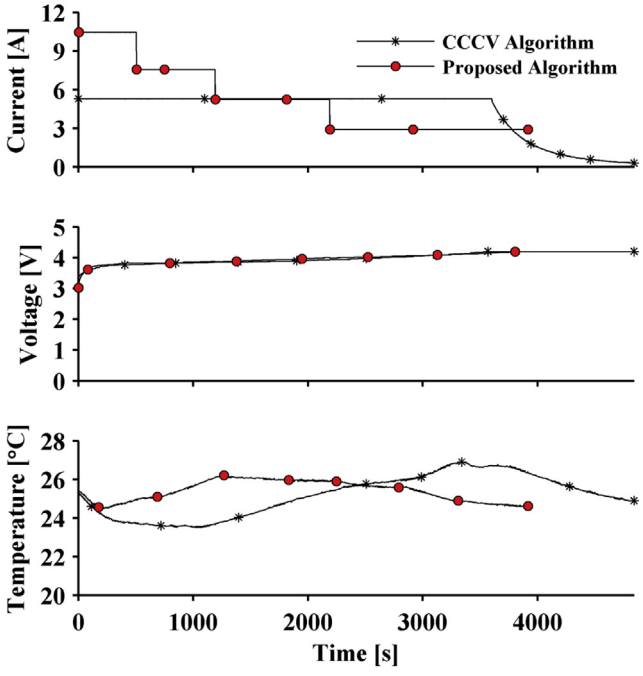

Fig. 13. Comparison between new charging strategy and CCCV charging method on LiPB B1.

Table 8
Experimental comparisons between proposed and CCCV charging method for different LiPBs.

LiPBs	Charging algorithm	Charged capacity (Ah)	Discharged capacity (Ah)	Energy eff. (%)	Charging time (s)	Temp. var. (°C)
B1 5.8 Ah	Proposed	5.75	5.66	96.22	3915	1.73
	CCCV	5.77	5.76	95.38	4838	3.4
B2 5.8 Ah	Proposed	5.55	5.49	95.39	3672	2.05
	CCCV	5.65	5.64	94.97	4768	3.27
B3 5.0 Ah	Proposed	4.74	4.64	95.57	3602	2.61
	CCCV	4.69	4.65	95.50	4561	3.18
B4 5.0 Ah	Proposed	4.76	4.66	94.30	3624	1.37
	CCCV	4.81	4.80	93.90	5162	3.21

4.3. Comparison with equivalent CCCV charging method

The experimental results of the new charging strategy are compared with those of the equivalent CCCV charging method to illustrate the performance. For the LiPBs (B1, B2, B3 and B4), the charging currents of the CC stage in the CCCV charging method are chosen as the average charging currents of the new charging strategy correspondingly and calculated form Eq. (27) which are 0.910 C, 0.936 C, 0.944 C and 0.942 C, respectively.

$$\mathrm{CC} = \frac{\sum_{m=1}^{4}(I_m \times T_m)}{\sum_{m=1}^{4} T_m} \tag{27}$$

where CC is the average charging current, I_m is the charging current in T_m charging duration for each charging stage in the new charging strategy.

The experimental results for 5.8 Ah LiPB (B1) are shown in Fig. 13. The charging time of the new charging strategy is shorter than that of the CCCV charging method (80 min) by 15 min, which is equivalent to 22.5%. The temperature variation of the new charging strategy is almost half of that of the CCCV method. To further demonstrate the merits of the new charging strategy, the experiments of the other three LiPBs (B2, B3 and B4) are also conducted and the corresponding results are summarised in Table 8. It can be seen that the new charging strategy achieves the similar better results to those obtained from B1 than the corresponding CCCV charging methods.

4.4. Application of proposed charging approach to other types of Li-ion batteries

The proposed charging strategy has been developed based on the observation of the experimental results as demonstrated in Section 2. If the other types of Li-ion batteries have the similar experimental results from the CCCV charging tests and the similar characteristics of the OCV versus the SOC to the batteries in this study, the proposed charging strategy should be able to apply for these types of Li-ion batteries.

5. Conclusions

The new charging strategy of the LiPBs is proposed based on the integration of Taguchi method (TM) and the SOC estimation. In the TM, the principle of the selection of charging current candidates, the formation of charging current patterns and the determination of the optimal charging current pattern is elaborated. In the SOC estimation, the procedure to design an adaptive switching gain sliding mode observer (ASGSMO) is explained in detail. The effectiveness of the new charging strategy has been verified by the experimental results of LiPBs and compared with the equivalent CCCV charging method. It shows that the new charging strategy can successfully charge the LiPB with different initial state of charges and the same type of LiPBs at different capacities and cycle life. Furthermore, it has the better performances (much shorter charging time, narrower temperature variation and slightly higher energy efficiency) than the equivalent CCCV charging method.

Acknowledgement

This research work is supported by Commonwealth of Australia, through the Cooperative Research Centre for Advanced Automotive Technology (AutoCRC) under the project of Electric Vehicle Control Systems and Power Management (C2-801).

References

[1] Z. Li, J. Huang, B.Y. Liaw, V. Metzler, J. Zhang, J. Power Sources 254 (2014) 168–182.
[2] N. Takami, H. Inagaki, Y. Tatebayashi, H. Saruwatari, J. Power Sources 244 (2013) 469–475.
[3] R. Gitzendanner, F. Puglia, C. Martin, D. Carmen, E. Jones, S. Eaves, J. Power Sources 136 (2004) 416–418.
[4] M. Alamgir, A.M. Sastry, SAE Int. (2008), 21-0017.
[5] A.A.H. Hussein, I. Batarseh, IEEE Trans. Veh. Technol. 60 (2011) 830–838.
[6] R.C. Cope, Y. Podrazhansky, in: Proc. of the 14th Battery Conference on Applications and Advances, USA, 1999, pp. 233–235.
[7] W.X. Shen, T.T. Vo, A. Kapoor, in: Proc. of the 6th International Conference on Industrial Electronics and Applications, Singapore, 2012, pp. 1567–1572.
[8] T. Ikeya, N. Sawada, J.I. Murakami, K. Kobayashi, M. Hattori, N. Murotani, S. Ujiie, K. Kajiyama, H. Nasu, H. Narisoko, Y. Tomaki, K. Adachi, Y. Mita, K. Ishihara, J. Power Sources 105 (2002) 6–12.
[9] J.H. Yan, H.Y. Chena, W.S. Li, C.I. Wang, Q.Y. Zhan, J. Power Sources 158 (2006) 1047–1053.
[10] H. Surmann, IEEE Trans. Ind. Electron. 43 (1996) 541–548.
[11] C.L. Liu, S. C Wang, Y.H. Liu, in: Proc. of the 6th International Conference on Soft Computing and Intelligent Systems and 13th International Symposium on Advanced Intelligent Systems, Japan, 2012, pp. 727–732.
[12] Y.H. Liu, J.H. Teng, Y.C. Lin, IEEE Trans. Ind. Electron. 52 (2005) 1328–1336.
[13] Y.H. Liu, Y.F. Luo, IEEE Trans. Ind. Electron. 57 (2010) 3963–3971.
[14] Y.H. Liu, C.H. Hsieh, Y.F. Luo, IEEE Trans. Energy Convers. 26 (2011) 654–661.
[15] X.P. Chen, W.X. Shen, Z.W. Cao, A. Kapoor, J. Power Sources 246 (2014) 667–678.
[16] J. lopez, M. Gonzalez, J.C. Viera, C. Blanco, in: Proc. of the 26th International Conference on Telecommunication Energy, USA, 2004, pp. 19–24.
[17] N. Omar, M.A. Monem, Y. Firouz, J. Salminen, J. Smekens, O. Hegazy, H. Gaulous, G. Mulder, P.V.D. Bossche, T. Coosemans, J.V. Mierlo, Appl. Energy 113 (2014) 1575–1585.
[18] B.M. Gopalsamy, B. Mondal, S. Ghosh, J. Sci. Ind. Res. 68 (2009) 686–695.
[19] T. Sivasakthivel, K. Murugesan, H.R. Thomas, Appl. Energy 116 (2014) 76–85.
[20] G.Y. Hwang, S.M. Hwang, H.J. Lee, J.H. Kim, K.S. Hong, W.Y. Lee, IEEE Trans. Magn. 41 (2005) 1900–1903.
[21] A. Awada, B. Wegmann, I. Viering, IEEE Trans. Veh. Technol. 60 (2011) 3825–3839.
[22] L.H. Chen, Comput. Operat. Res. 24 (1997) 937–944.
[23] A. Al-Refaie, T.H. Wu, M.H. Li, Jordan J. Mech. Ind. Eng. 4 (2010) 314–323.
[24] R.K. Roy, Design of Experiments Using Taguchi Approach: 16 Steps to Product and Process Improvement, John Wiley & Son, Inc, 2001.
[25] P.J. Cheng, C.H. Cheng, S.B. Hong, in: Proc. of the International Conference on Advanced Robotics and Intelligent Systems, Taiwan, 2013, pp. 70–75.
[26] X.P. Chen, W.X. Shen, Z.W. Cao, A. Kapoor, Comput. Chem. Eng. 64 (2014) 114–123.
[27] M. Chen, A. Gabriel, M. Rincon, IEEE Trans. Energy Convers. 21 (2006) 504–511.
[28] H. He, R. Xiong, J. Fan, Energies 4 (2011) 582–598.
[29] X. Hu, S. Li, H. Peng, J. Power Sources 198 (2012) 359–367.